Topological invariants for interacting topological insulators. II. Breakdown of single-particle Green's function formalism

Yuan-Yao He,[1] Han-Qing Wu,[1] Zi Yang Meng,[2] and Zhong-Yi Lu[1]
[1]*Department of Physics, Renmin University of China, Beijing 100872, China*
[2]*Beijing National Laboratory for Condensed Matter Physics, and Institute of Physics, Chinese Academy of Sciences, Beijing 100190, China*
(Received 26 December 2015; revised manuscript received 29 March 2016; published 31 May 2016)

Topological phase transitions in free fermion systems can be characterized by the closing of single-particle gap and the change in topological invariants. However, in the presence of electronic interactions, topological phase transitions can be more complicated. In paper I of this series [Phys. Rev. B **93**, 195163 (2016)], we have proposed an efficient scheme to evaluate the topological invariants based on the single-particle Green's function formalism. Here, in paper II, we demonstrate several interaction-driven topological phase transitions (TPTs) in two-dimensional (2D) interacting topological insulators (TIs) via large-scale quantum Monte Carlo (QMC) simulations, based on the scheme of evaluating topological invariants presented in paper I. Across these transitions, the defining symmetries of the TIs have been neither explicitly nor spontaneously broken. In the first two models, the topological invariants calculated from the Green's function formalism succeed in characterizing the topologically distinct phases and identifying interaction-driven TPTs. However, in the other two models, we find that the single-particle gap does not close and the topological invariants constructed from the single-particle Green's function acquire no change across the TPTs. Unexpected breakdown of the Green's function formalism in constructing the topological invariants is thus discovered. We thence classify the topological phase transitions in interacting TIs into two categories in practical computation: Those that have noninteracting correspondence can be characterized successfully by the topological invariants constructed from the Green's functions, while for the others that do not have noninteracting correspondence, the Green's function formalism experiences a breakdown, but more interesting and exciting phenomena, such as emergent collective critical modes at the transition, arise. Discussion on the success and breakdown of topological invariants constructed from the Green's function formalism in the context of symmetry protected topological (SPT) states is presented.

DOI: 10.1103/PhysRevB.93.195164

I. INTRODUCTION

This is paper II of the series on "topological invariants for interacting topological insulators." In paper I of this series [1], we have proposed an efficient scheme to evaluate the topological invariants based on single-particle Green's function formalism. By introducing an interpolation process we have successfully overcome the ubiquitous finite-size effect of topological invariants in QMC simulations of interacting TIs and obtained ideally quantized spin Chern number in one-body-parameter-driven topological phase transition between TIs (or between TI and topologically trivial insulators). In this paper, we apply the numerical evaluation scheme developed in paper I to wider classes of interacting TIs, where across the interaction-driven topological phase transitions, the defining symmetries of the topological insulators have been neither explicitly nor spontaneously broken, but the topological invariants constructed from the Green's function may experience unexpected breakdown. Thus, even though there are cases where the interaction-driven TPTs can be successfully captured by the Green's function scheme, we found that in several TPTs the topological invariants fail and provide artificial information about the transition, as well as the phases. We attribute such difference to the fact that in cases where the Green's function formalism works, the phases across the interaction-driven TPT have noninteracting correspondence, but in the cases where the Green's function formalism fails, there is no noninteracting correspondence to the phases after the interaction-driven TPT. Consequently, calling for more complete understanding of topological invariants in interacting TIs is clearly manifested.

As discussed in paper I [1], for noninteracting TIs, both Z_2 invariant [2,3] and spin Chern number [4] can be simply evaluated from Hamiltonian matrix. For example, in systems with spatial inversion symmetry, the Z_2 invariant can be calculated as products of parity eigenvalues of all occupied bands at time-reversal invariant (TRI) points in the Brillouin zone (BZ) [3]. Spin Chern number can be calculated by integrating the Berry curvature over BZ [5]. For interacting TIs, numerical evaluations of the topological invariants become more involved. The generalizations of constructing topological invariants from single-particle Green's function [5–11] and twisted boundary phases [12,13] have been proposed respectively, whereas the former and in particular its zero-frequency version, has been systematically developed in Refs. [10,14–17]. There are successful applications of the Green's function formalism in the one-dimensional (1D) Su-Schrieffer-Heeger model [18], in the two-dimensional (2D) Kane-Mele-Hubbard model with various generalizations [1,19–23], in the Bernevig-Hughes-Zhang model [24–26], and also in real material calculations with LDA+Gutzwiller and LDA+DMFT where SmB_6 [27] and PuB_6 [28] have been predicted to be realizations of correlated TIs from calculating Z_2 invariant.

However, this is just the tip of the iceberg. The interplay between topology and electronic interaction is expected to lead to more complicated and richer physics. Many possible generalizations of the concept of TI to interacting systems have been put forward. Many exotic phenomena of interacting TIs

have been predicted/discovered, such as topological Kondo insulator [27–31], topological Mott insulator and fractionalized TI in 2D and 3D systems [32,33], interaction-reduced classification of noninteracting TIs in the 10 distinct classes (the tenfold way [34–36]) in 1D, 2D, and 3D systems [37–49], and interaction-driven intrinsic topological order at the boundary of TIs [43,50–57]. Besides fermionic systems, it was proposed that bosonic systems can also form exotic states that are similar to fermionic TIs [40,50,58–60], all of which are generally called symmetry protected topological (SPT) states.

More recently, an exotic interaction-driven TPT in the 2D system (the BKMH-J model below) that is fundamentally different from the TI-to-trivial insulator transition in noninteracting systems, was discovered with large-scale QMC simulations [61,62]. Across the transition, fermions never close their gap, but emergent collective bosonic modes become critical. Thus one can view this transition as a transition between a bosonic SPT state and a trivial featureless Mott insulator [62,63]. Within appropriate parameter region, this transition is described by a $(2+1)$D $O(4)$ nonlinear sigma model with exact $SO(4)$ symmetry, and a topological term at exactly $\Theta = \pi$. It was proposed that there is a series of such interaction-driven TPT in 2D interacting TIs [63], and they can be studied with unbiased QMC simulations without minus-sign problem (the BKMH-J and BKMH-V models discussed here are among them). A natural question then arises, namely, what will be the fate of the topological invariants constructed from single-particle Green's function formalism across these exotic interaction-driven TPTs. Here, in this paper, we provide the answer.

In this paper, employing large-scale QMC simulations, we explore several interaction-driven TPTs in 2D TIs with neither explicit nor spontaneous symmetry breaking. These TPTs happen in the generalized Kane-Mele-Hubbard model [1,19–21] (GKMH), cluster Kane-Mele-Hubbard model [1,23,64] (CKMH), the bilayer Kane-Mele-Hubbard model (BKMH) with interlayer antiferromagnetic spin-spin interaction J (BKMH-J) [62], and interlayer interaction V (BKMH-V). The TPTs in the first two models have noninteracting correspondences, and by means of the interpolation process developed in paper I [1], we obtain the ideally quantized topological invariants (spin Chern number) to characterize them. The TPTs in the second two models do not have noninteracting analogues, we found an unexpected breakdown of the Green's function formalism in constructing the topological invariants, in which it is clearly seen that after the interaction-driven TPTs, the trivial insulators [product states of $SO(4)$ interlayer J-singlet or V-singlet] are still incorrectly associated with ideally quantized, nonzero spin Chern numbers if they were constructed from single-particle Green's function. These artificial results show the limitation of the single-particle Green's function formalism in monitoring interaction-driven TPTs and highlight calling for more complete understanding and versatile technique in studying interacting TIs.

The rest of the paper is organized as follows. In Sec. II, the QMC results of the interaction-driven TPTs are presented, containing the ones in GKMH and CKMH models which have noninteracting correspondences and the Green's function formalism succeeds, and the others in BKMH-J and BKMH-V models which do not have noninteracting analogues and the Green's function formalism fails. In Sec. III, we carry out detailed analysis for the reason of the breakdown of spin Chern number constructed from Green's function formalism in characterizing certain interaction-driven TPTs. Finally, a summary is given in Sec. IV.

II. NUMERICAL RESULTS

In this section, we present the QMC simulation results for the four interaction-driven TPTs with neither explicit nor spontaneous symmetry breaking, with special focus on the numerical data of topological invariants calculated from the zero-frequency single-particle Green's function. As for the Green's function formalism in constructing the topological invariants, the interpolation process to overcome the finite size effect in QMC simulation, and the basic introduction of the projector QMC technique itself, the readers are referred to paper I [1].

A. Interaction-driven TPTs in GKMH model

As introduced in paper I [1], the generalized Kane-Mele-Hubbard (GKMH) model [19–21] is given by

$$\begin{aligned}\hat{H} = &-\sum_{\langle i,j\rangle\sigma} t_{ij}(c^\dagger_{i\sigma}c_{j\sigma} + \text{H.c.}) - t_3\sum_{\langle\langle\langle i,j\rangle\rangle\rangle\sigma}(c^\dagger_{i\sigma}c_{j\sigma} + \text{H.c.}) \\ &+ i\lambda\sum_{\langle\langle i,j\rangle\rangle\alpha\beta} v_{ij}(c^\dagger_{i\alpha}\sigma^z_{\alpha\beta}c_{j\beta} - c^\dagger_{j\beta}\sigma^z_{\beta\alpha}c_{i\alpha}) \\ &+ \frac{U}{2}\sum_i (n_{i\uparrow} + n_{i\downarrow} - 1)^2 \\ &+ \frac{J}{8}\sum_{\langle i,j\rangle}[(D_{i,j} - D^\dagger_{i,j})^2 - (D_{i,j} + D^\dagger_{i,j})^2], \end{aligned} \tag{1}$$

where $D_{i,j} = \sum_\sigma c^\dagger_{i\sigma}c_{j\sigma}$. For the nearest-neighbor (NN) hopping, we have $t_{ij} = t_d$ for the NN bonds inside unit cells and $t_{ij} = t$ for the others, as shown in Fig. 1(a). The t_3 term is the third-nearest-neighbor hopping. The λ term represents spin-orbit coupling (SOC) connecting the next-nearest-neighbor sites with a complex (time-reversal symmetric) hopping with amplitude λ. The factor $v_{ij} = v_{ji} = \pm 1$ depends on the orientation of the two nearest-neighbor bonds that an electron moves in going from site i to j. The U term is the on-site Coulomb repulsion, while the J term, which only exists for the NN bonds inside unit cells, is a faithful approximation [62] of the antiferromagnetic (AFM) Heisenberg interaction $J\sum_{\langle ij\rangle}\mathbf{S}_i\cdot\mathbf{S}_j$. Throughout this paper, we set t as the energy unit. The honeycomb lattice and its BZ are shown in Figs. 1(a) and 1(b).

Due to $U(1)_{\text{spin}} \times U(1)_{\text{charge}} \rtimes Z_2^T$ symmetry, the GKMH model without interaction belongs to $\mathbb{Z}$ classification. Figure 1(c) shows the $(t_d/t) - (t_3/t)$ phase diagram for $\lambda/t > 0$, determined from both Z_2 invariant $(-1)^\nu$ and spin Chern number C_s. Here the phase boundaries is independent of λ/t parameter as long as $\lambda/t > 0$. As we see, there are four different phases with different spin Chern number C_s, in which three of them with spin Chern numbers $C_s \neq 0$ are topologically nontrivial and the last one with $C_s = 0$ is trivial.

Here we concentrate on two U-driven TPTs, which are described by spin Chern number variation in odd or even

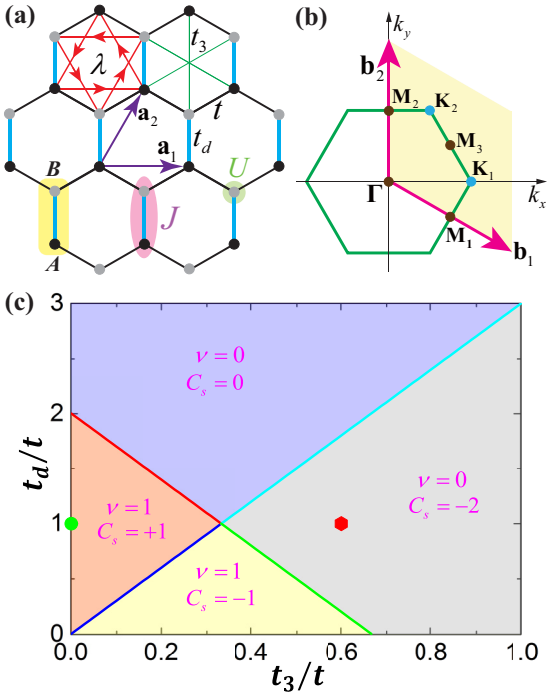

FIG. 1. (a) Illustration of honeycomb lattice and all the terms in GKMH model as Eq. (1). The unit cell is presented as the yellow shaded rectangle, consisting of A and B sublattices denoted by black and gray circles. The lattice is spanned by primitive vectors $\mathbf{a}_1 = (\sqrt{3},0)a$, $\mathbf{a}_2 = (1/2,\sqrt{3}/2)a$ with a the lattice constant. The black and blue lines denotes nearest-neighbor hopping between (t) and inside (t_d) unit cells, while the SOC term (λ) and third-neighbor hopping (t_3) are represented by red and green lines. The arrows in red lines shows $v_{ij} = +1$ for the spin-up part. The on-site U interaction and the AFM J interaction existing only inside the unit cell are presented by green circles and magenta ellipse. (b) The BZ of GKMH model. $\mathbf{K}_1$,$\mathbf{K}_2$ are Dirac points, while Γ, $\mathbf{M}_1$, $\mathbf{M}_2$, $\mathbf{M}_3$ are the four TRI points. (c) The noninteracting $(t_d/t) - (t_3/t)$ phase diagram for GKMH model, and the Z_2 invariant $(-1)^\nu$ and spin Chern number C_s for all the phases. The green dot ($t_d = t, t_3 = 0$) and red hexagon ($t_d = t, t_3 = 0.6t$) along with $\lambda = 0.2t$ and $J = 1$ are the chosen parameters, based on which we identify the U-driven TPTs in Fig. 2 and Fig. 3, respectively.

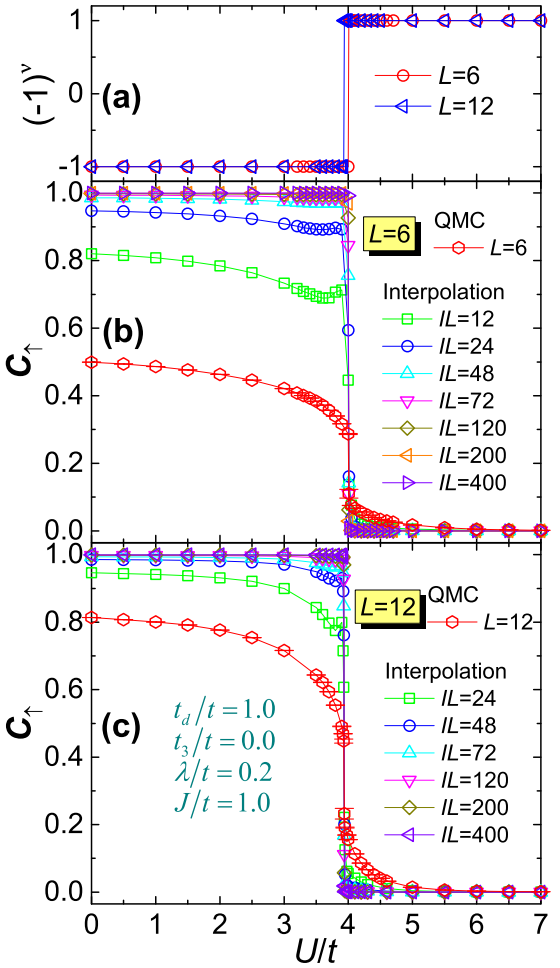

FIG. 2. (a) Z_2 invariant $(-1)^\nu$ and (b), (c) Chern number $C_\uparrow$ for the U-driven topological phase transition in GKMH model with $t_d = t, \lambda = 0.2t, t_3 = 0$ [green dot in Fig. 1(c)] and $J = t$ from QMC results for $L = 6$ and $L = 12$ and interpolation to large IL. We can observe that Z_2 invariant $(-1)^\nu$ are integer quantized. The Chern number $C_\uparrow$ obtained from finite size systems $L = 6,12$ acquire a jump with finite value at the transition point, but the jump is not ideally quantized due to finite size effect. After interpolation, based on the $L = 6,12$ QMC data, the ideally quantized Chern number is achieved.

integer across the transitions. The anisotropy introduced by the J term inside the unit cell suppresses the xy-AFM long range order, which otherwise arises in the large U limit with $J = 0$ [65–68], but favors a topologically trivial dimerized insulator phase without breaking time-reversal symmetry and spin $U(1)$ symmetry. The U-driven TPT with spin Chern number variation $|\Delta C_s| = 1$ can be realized by setting $t_d = t, \lambda = 0.2t, t_3 = 0$ [green dot in Fig. 1(c)], $J = t$ and increasing U. The other U-driven TPT with $|\Delta C_s| = 2$ appears by choosing $t_d = t, \lambda = 0.2t, t_3 = 0.6t$ [red hexagon in Fig. 1(c)], $J = t$. For both phase transitions, the possible intervening xy-AFM long-range order is excluded by extrapolating the corresponding magnetic structure factor to thermodynamic limit. Thus, there is no spontaneous symmetry breaking during the transitions. We also need to emphasize that such interaction-driven TPTs can exist for a fairly large range of parameters, as long as the intervening xy-AFM order is absent, and we only demonstrate the above two representative cases.

For the TPT with $|\Delta C_s| = 1$ in the GKMH model, the results of both Z_2 invariant and spin Chern number C_s are shown in Fig. 2. The integer-quantized Z_2 invariant determines the interaction-driven TPT with $U_c \approx 4.005t$ for the $L = 6$ system and $U_c \approx 3.935t$ for the $L = 12$ system, as shown in Fig. 2(a), which indicates a very small finite-size effect in the topological phase transition point. We find that across the transition both the parity changing and the single-particle gap closing only happen at the $\mathbf{M}_2$ point in the BZ, which is due to the anisotropy introduced by the J term. However, the Chern number $C_\uparrow$ calculated from finite size systems $L = 6,12$ shown in Figs. 2(b) and 2(c) suffers from severe finite-size effect, meanwhile the value and jump in C_s are far from ideal quantization, even though its finite-value jumps happen at the

transition points. We then apply the interpolation process [1] to obtain its integer-quantized values. The results are also shown in Figs. 2(b) and 2(c). We have carried out interpolation for QMC results on $L = 6$ [Fig. 2(b)] and $L = 12$ [Fig. 2(c)] systems and the interpolation lattice size IL can be as large as $IL = 400$. The convergence of $C_\uparrow$ with IL to its expected integer value can be clearly observed.

Combining the Z_2 invariant $(-1)^\nu$ and spin Chern number $C_s = C_\uparrow$ in Fig. 2, the U-driven, QSH insulator to dimer insulator transition is clearly established. In the dimer insulator phase, spin singlets are formed on the bonds inside unit cell due to presence of J and U interactions. Under the dimer limit, the system is actually a direct product state, which is topologically trivial ($C_s = 0$) since all the electronic degrees of freedom are frozen, and there is no edge state even if open boundary was created. This trivial dimer insulator is adiabatically connected—without going through phase transition and symmetry breaking—to the $\nu = 0, C_s = 0$ noninteracting trivial insulator in Fig. 1(c), while the interacting quantum spin Hall (QSH) insulator at $J = 1$ and $U < 4t$ with $C_s = 1$ is adiabatically connected to the $\nu = 1, C_s = +1$ phase in Fig. 1(c). This means that the above U-driven TPT with $|\Delta C_s| = 1$ has a noninteracting correspondence which is the transition at the red line in Fig. 1(c), and the effect of interactions is only to renormalize the hopping parameters.

For the TPT with $|\Delta C_s| = 2$ in the GKMH model, the results of spin Chern number C_s are shown in Fig. 3, for both finite size QMC and interpolation results. Without interaction, the system is a TI with $C_s = -2$, for which the Z_2 invariant is $\nu = 0$ as $(-1)^\nu = +1$. With $J = t$ and increasing U, a U-driven TPT from $C_s = -2$ TI to $C_s = 0$ dimer insulator is expected. Across this TPT, we observe that the single-particle gap closing and the parity change happen at both $\mathbf{M}_1$ and $\mathbf{M}_3$ points, although the total Z_2 parity does not have a variation. Combining the jumps in both parity and Chern number $C_\uparrow$ with the gap closing behavior, we determine the transition points for this TPT as $U_c \approx 3.46(5)t$ for $L = 6$ and $U_c \approx 3.30(5)t$ for $L = 12$, which gives a $\Delta U_c \approx 0.16t$ shift of the phase boundary due to finite size effect in QMC.

To reach ideally quantized spin Chern number for this U-driven TPT, the interpolation process is then applied. The calculation results of Chern number $C_\uparrow$ after the interpolation from $L = 6, 12$ systems are also shown in Figs. 3(a) and 3(b). Again, we achieve the ideally quantized Chern number $C_\uparrow$ and a sharp transition from $C_s = -2$ to $C_s = 0$ when the interpolation lattice size IL is large enough. There are some nonmonotonic behaviors in the results for small IL. These behaviors are caused by the τ cutoff that we applied in the interpolation [1], but they disappear when IL is large enough.

Similar to the $|\Delta C_s = 1|$ case, this U-driven TI-dimer TPT with $|\Delta C_s| = 2$ also has noninteracting correspondence. The $C_s = -2$ TI phase at $J = t$ and $U < 3.5$ is adiabatically connected to the $\nu = 0, C_s = -2$ TI phase in Fig. 1(c), while the $\nu = 0, C_s = 0$ dimer-singlet insulator at $J = t$ and $U > 3.5$ is adiabatically connected to the $\nu = 0, C_s = 0$ phase in Fig. 1(c) as well. So the U-driven TPT in Fig. 3 is exactly the same as the transitions on the solid cyan line in Fig. 1(c). Considering both TPTs with $|\Delta C_s| = 1$ and $|\Delta C_s| = 2$, it's interesting that the spin Chern number constructed from

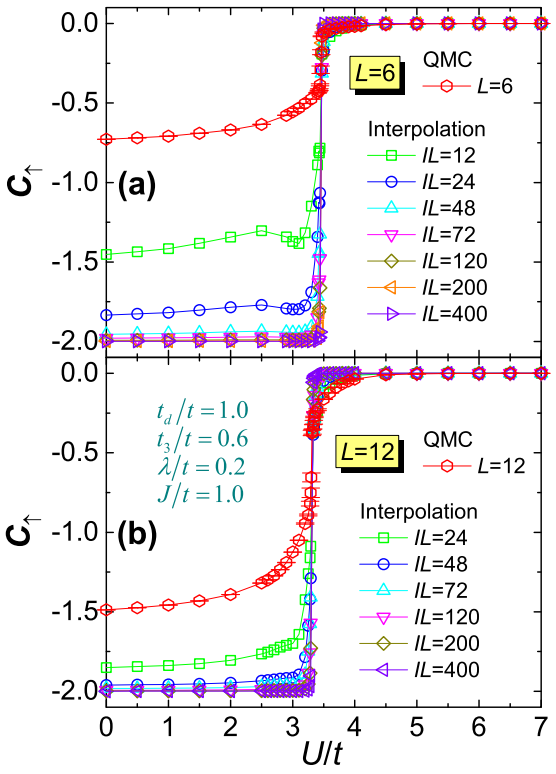

FIG. 3. (a), (b) Chern number $C_\uparrow$ for the U-driven topological phase transition in the GKMH model with $t_d = t, \lambda = 0.2t, t_3 = 0.6t$ [red hexagon in Fig. 1(c)] and $J = t$ from finite-size calculations by QMC method for $L = 6$ and $L = 12$ systems and interpolation with large IL. For finite size system, the Chern number $C_\uparrow$ acquires a jump with finite value which is not quantized at the transition point, after the interpolation, the convergence to the ideally quantized Chern number is clearly seen and it sharply defines the interaction-driven topological phase transition.

single-particle Green's function can detect interaction-driven TPTs, even though interaction U for both transitions is large. Clearly, this is due to the fact that these TPTs have noninteracting correspondences.

B. Interaction-driven TPTs in CKMH model

As introduced in paper I [1], the CKMH model [23,64] has six lattice sites per unit cell, and the model Hamiltonian is given by

$$\begin{aligned}\hat{H} = &-\sum_{\langle ij\rangle\sigma} t_{ij}(c^\dagger_{i\sigma}c_{j\sigma} + c^\dagger_{j\sigma}c_{i\sigma}) \\ &+ i\lambda_I \sum_{\langle\langle ij\rangle\rangle\alpha\beta} v_{ij}(c^\dagger_{i\alpha}\sigma^z_{\alpha\beta}c_{j\beta} - c^\dagger_{j\beta}\sigma^z_{\beta\alpha}c_{i\alpha}) \\ &+ i\lambda_O \sum_{\langle\langle ij\rangle\rangle\alpha\beta} v_{ij}(c^\dagger_{i\alpha}\sigma^z_{\alpha\beta}c_{j\beta} - c^\dagger_{j\beta}\sigma^z_{\beta\alpha}c_{i\alpha}) \\ &+ \frac{U}{2}\sum_i (n_{i\uparrow} + n_{i\downarrow} - 1)^2 \,. \end{aligned} \tag{2}$$

For the nearest-neighbor (NN) hopping, we have $t_{ij} = t$ for the NN bonds inside unit cells and $t_{ij} = t_d$ for those connecting the six-site unit cells, as shown in Fig. 4(a). λ_I and λ_O are

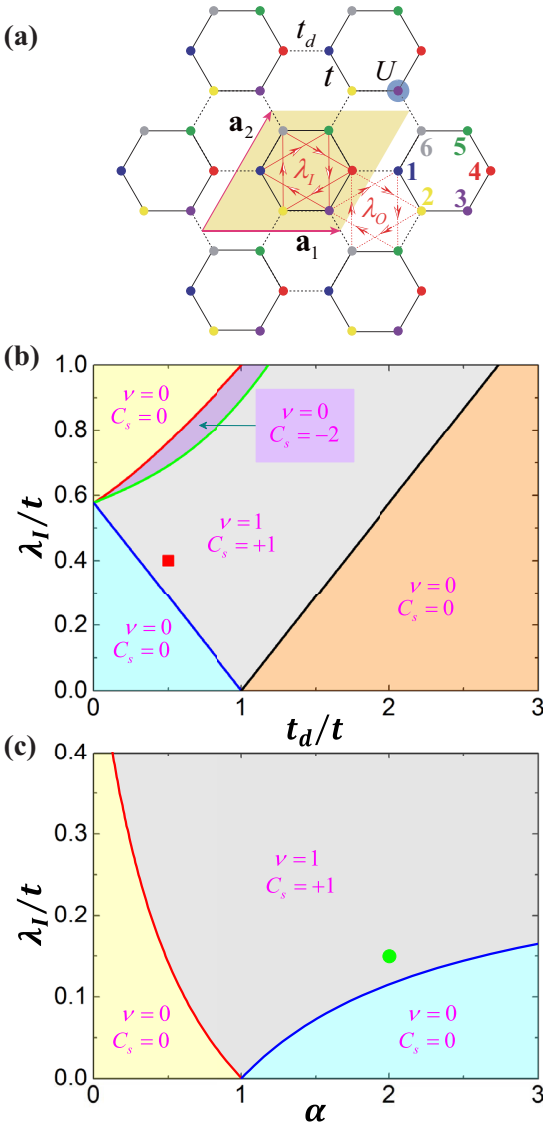

FIG. 4. (a) The CKMH model with six site unit cell. The yellow shaded region shows the unit cell with primitive lattice vectors $\mathbf{a}_1=(\sqrt{3},0)a, \mathbf{a}_2=(1/2,\sqrt{3}/2)a$ while the distance between nearest-neighbor lattice sites is $a/\sqrt{3}$. The black solid and dotted lines indicate the nearest-neighbor hopping terms inside and between different unit cells. The red solid and dotted lines represent the SOC terms inside and between different unit cells. The sign choice for SOC hopping is the same as that in Fig. 1(a). The on-site Coulomb repulsion is shown by the blue shaded circle. (b) The noninteracting $(t_d/t)-(\lambda_I/t)$ phase diagram for the CKMH model with $\lambda_O=0$. (c) The noninteracting $\alpha-(\lambda_I/t)$ phase diagram for the CKMH model. The red square $(t_d/t=0.5,\lambda_I/t=0.4)$ and green dot $(\alpha=0.5,\lambda_I/t=0.15)$ are the chosen parameters based on which the U-driven TPTs are studied in Figs. 5 and 6, respectively.

the SOC terms inside and between unit cells, respectively. U is the on-site Coulomb repulsion. Similar to the GKMH model, the CKMH model preserves $U(1)_{\text{spin}}\times U(1)_{\text{charge}}\rtimes Z_2^T$ symmetry, which also results in $\mathbb{Z}$ classification. Besides, both spatial inversion symmetry and particle-hole symmetry are also conserved in CKMH model. The hexagonal BZ of the CKMH model differs with that of the GKMH model in Fig. 1(b) only up to a rescaling of reciprocal lattice vectors.

Similar to the CKMH model discussed in paper I [1], we first set $\lambda_O=0$ and only keep the SOC term λ_I finite. In this case, the $(t_d/t)-(\lambda_I/t)$ phase diagram of the noninteracting CKMH model is shown in Fig. 4(b). We can observe that two TIs exist in the middle region of the phase diagram, with different spin Chern numbers $C_s=+1$ at small λ_I and $C_s=-2$ at larger λ_I. Then, we keep all three hopping parameters t_d, λ_I, and λ_O finite and introduce a ratio of $\alpha=t_d/t=\lambda_O/\lambda_I$. The noninteracting $\alpha-(\lambda_I/t)$ phase diagram is presented in Fig. 4(c).

In the CKMH model, a large on-site U interaction can drive the system into a topologically trivial insulator without spontaneous symmetry breaking, i.e., without AFM long range order, provided that the value of t_d/t is far away from 1. As will become clear below, these trivial insulators can be either a plaquette valance bond solid (pVBS) or columnar valance bond solid (cVBS) [69]. These VBSs are insulators built from spin singlets, with either two electrons or six electrons. In the following, we first study the U-driven TPT with $t_d=0.5t,\lambda_I=0.4t$ [red square in Fig. 4(b)], and then the U-driven TPT with $\alpha=2,\lambda_I=0.15t$ [green dot in Fig. 4(c)].

We first study the U-driven TPT marked by the red square $t_d=0.5t,\lambda_I=0.4t$ in Fig. 4(b). Results of both Z_2 invariant $(-1)^\nu$ and Chern number $C_\uparrow$ from the QMC data with $L=6,12$ and interpolation with large IL are presented in Fig. 5. Both the integer variation of Z_2 invariant [Fig. 5(a)] and finite value jump of Chern number $C_\uparrow$ [Figs. 5(b) and 5(c)] suggest the TPT at $U_c\approx 3.085t$ for $L=6$ system and $U_c\approx 3.125t$ for $L=12$ system. Across the transition, we find that both single-particle gap closing and parity change happen at Γ point. To obtain the ideally quantized Chern number $C_\uparrow$, the interpolation process is applied, as shown in Figs. 5(b) and 5(c). The quantized $C_\uparrow$ results in Figs. 5(b) and 5(c) further confirm the U-driven TPT with spin Chern number variation $|\Delta C_s|=1$.

The topologically trivial phase after the TPT is a pVBS, in which six electrons form a total spin singlet inside a unit cell indicated by the yellow shaded region in Fig. 4(a). This phase is easy to understand. With large U, the effective model of the system becomes $J-J'$ Heisenberg model in which J,J' are inside and between different unit cells with $J\propto t^2/U$ and $J'\propto t_d^2/U$, respectively. For the parameter $t_d=0.5t$, we arrive at approximately $J\approx 4J'$ (neglecting the contribution of SOC hopping term), such a $J-J'$ Heisenberg model acquires a pVBS ground state on the honeycomb lattice [69]. Thus this TPT is a U-driven QSH-to-pVBS transition. What's more, the $(-1)^\nu=-1,C_s=+1$ QSH insulator at $U<3$ in the CKMH model is adiabatically connected to the $\nu=1,C_s=+1$ gray-colored QSH region in the noninteracting phase diagram Fig. 4(b). In contrast, the $(-1)^\nu=+1,C_s=0$ phase for $U>3$ is adiabatically connected to the $\nu=0,C_s=0$ phase in the cyan region in Fig. 4(b). Hence the TPT shown in Fig. 5 is exactly the same as the transition along the blue solid line in the noninteracting phase diagram Fig. 4(b).

We then study the U-driven TPT in CKMH model starting from the green dot $\alpha=2,\lambda_I=0.15t$ in Fig. 4(c). Results of both Z_2 invariant $(-1)^\nu$ and Chern number $C_\uparrow$ calculated from the QMC data in $L=6,12$ systems and interpolation

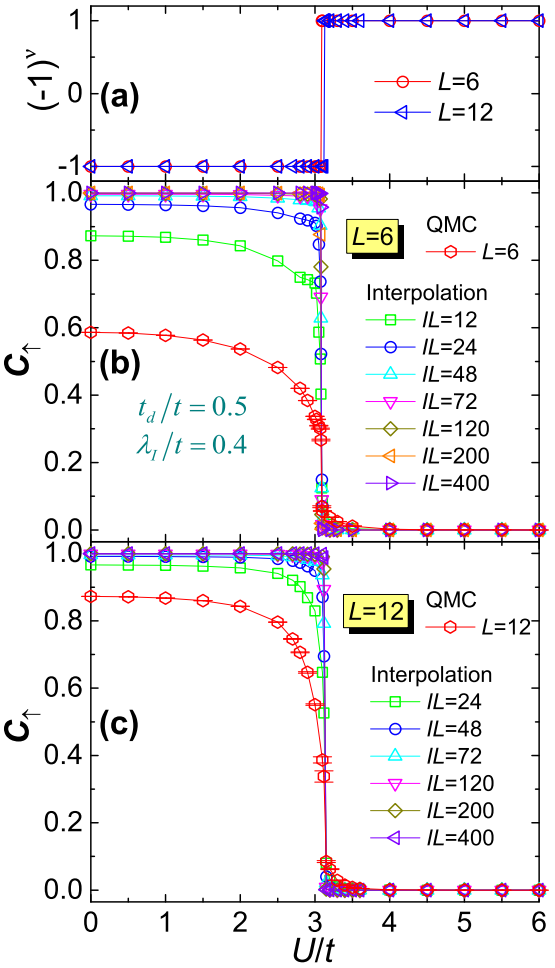

FIG. 5. (a) Z_2 invariant $(-1)^{\nu}$ and (b), (c) Chern number $C_{\uparrow}$ for the U-driven topological phase transition in the CKMH model with $t_d = 0.5t, \lambda_I = 0.4t$ [red square in Fig. 4(b)] from QMC calculation for $L = 6,12$ system and interpolation with large IL. Across the TPT point, the quantized Z_2 invariant experiences an integer variation and Chern number $C_{\uparrow}$ acquires a finite-value jump. After the interpolation with the QMC data in $L = 6,12$ with large IL, the Chern number $C_{\uparrow}$ reaches its ideally quantized value.

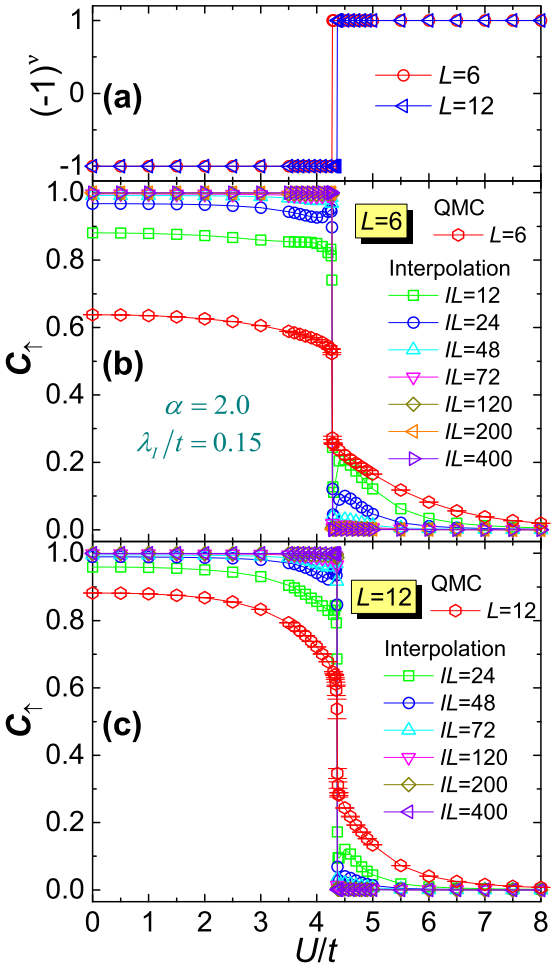

FIG. 6. (a) Z_2 invariant $(-1)^{\nu}$ and (b), (c) Chern number $C_{\uparrow}$ for the U-driven topological phase transition in the CKMH model with $\alpha = 2, \lambda_I = 0.15t$ [green dot in Fig. 4(c)] from QMC calculation for $L = 6,12$ systems and interpolation with large IL. Across the TPT, the quantized Z_2 invariant experiences an integer variation and Chern number $C_{\uparrow}$ acquires a finite-value jump. After the interpolation, the Chern number $C_{\uparrow}$ reaches ideally quantized value and demonstrates the interaction-driven TPT.

with large IL are, respectively, shown in Figs. 6(a), 6(b), and 6(c). Both these two topological invariants experience jumps at $U_c \approx 4.275t$ for $L = 6$ system and $U_c \approx 4.365t$ for $L = 12$ system, suggesting the transition point $U_c \approx 4.37t$. Across the transition, we also observe that the single-particle gap closing and parity change happen at the Γ point. Likewise, the interpolation scheme, applied upon the QMC data in $L = 6$ and $L = 12$ systems, gives the ideally quantized C across this TPT, as shown in Figs. 6(b) and 6(c).

With $\alpha = 2, \lambda_I = 0.15t$, at large U limit, in the effective $J - J'$ model, we now have $J' > J$, so the ground state of CKMH model at $U > 4.4$ is a cVBS state [69], in which the spin singlets form on the t_d bonds in Fig. 4(a) connecting different unit cells. Similar to the CKMH model with $t_d = 0.5t, \lambda_I = 0.4t$ discussed above, the $(-1)^{\nu} = -1, C_s = +1$ phase at $U < 4.4$ is adiabatically connected to the gray-colored $\nu = 1, C_s = +1$ QSH region in the noninteracting phase diagram Fig. 4(c), while the cVBS phase at $U > 4.4$ is adiabatically connected to the $\nu = 0, C_s = 0$ phase with light cyan color in Fig. 4(c). So this U-driven QSH-to-cVBS TPT is the same as the transition on the blue solid line in Fig. 4(c).

C. Interaction-driven TPT in the BKMH-J model

The next two interaction-driven TPTs are very different from those discussed above in that from here we will observe breakdown of the topological invariants constructed from the Green's function formalism and find a new type of interaction-driven TPT where the fermions are gapped throughout the TPT but there are emergent collective bosonic modes that become critical at the transition. The topological trivial phases after the TPT are featureless Mott insulators, which do not have noninteracting correspondences.

Let's begin with the bilayer Kane-Mele-Hubbard model with interlayer AFM interaction J [61–63]. The Hamiltonian

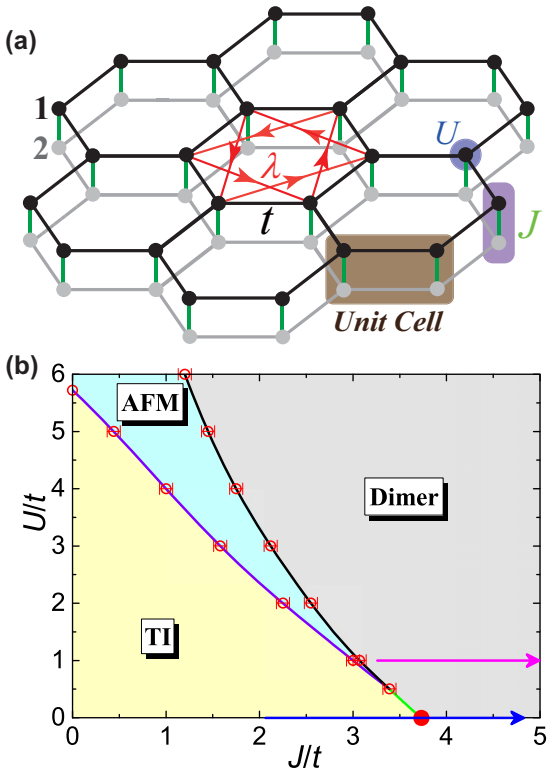

FIG. 7. (a) Illustration of AA-stacked honeycomb lattice and bilayer KMH model with interlayer AFM interaction J. The four-site unit cell is presented as the shaded rectangle. The gray and black lines indicates the nearest-neighbor hopping t on layers 1 and 2, respectively. The spin-orbital coupling term λ, for one spin flavor, is shown by the red lines and arrows with $v_{ij} = +1$. The on-site Coulomb repulsion U and interlayer AFM coupling J are represented by the shaded circle and rectangle. (b) The U-J phase diagram for BKMH-J model for $\lambda = 0.2t$. The blue and magenta lines with arrow demonstrate the paths where the topological invariants constructed from Green's function are calculated in Figs. 8 and 9, respectively.

of the BKMH-J model is given as

$$\begin{aligned} H = & -t \sum_{\xi\langle i,j\rangle,\alpha} (c^\dagger_{\xi i\alpha} c_{\xi j\alpha} + c^\dagger_{\xi j\alpha} c_{\xi i\alpha}) \\ & + i\lambda \sum_{\xi\langle\langle i,j\rangle\rangle,\alpha\beta} v_{ij} (c^\dagger_{\xi i\alpha} \sigma^z_{\alpha\beta} c_{\xi j\beta} - c^\dagger_{\xi j\beta} \sigma^z_{\beta\alpha} c_{\xi i\alpha}) \\ & + \frac{U}{2} \sum_{\xi i} (n_{\xi i} - 1)^2 \\ & + \frac{J}{8} \sum_i [(D_{1i,2i} - D^\dagger_{1i,2i})^2 - (D_{1i,2i} + D^\dagger_{1i,2i})^2], \end{aligned} \quad (3)$$

where $\xi = 1,2$ is the layer index. Inside each layer, the nearest-neighbor hopping t and SOC term λ are the same as those in the GKMH model. The interactions include the on-site Coulomb repulsion U and interlayer AFM exchange coupling J, which has the same expression as the J interaction term in Eq. (1), except that now the J term is the interlayer one. The lattice geometry and all the terms in the BKMH-J Hamiltonian are presented in Fig. 7(a). Its unit cell contains four lattice sites, and the corresponding BZ is the same as that in Fig. 1(b).

The BKMH-J model has $U(1)_{\text{spin}} \times [U(1) \times U(1)]_{\text{charge}} \rtimes Z_2^T$ symmetry. Here the two $U(1)$ charge symmetries correspond to the charge conservations in each layer. The detailed U-J phase diagram of the BKMH-J model has already been carefully studied in Ref. [62] by the QMC simulations. With finite λ and no interaction $U = J = 0$, the system is a TI with spin Chern number $C_s = +2$ and Z_2 invariant $(-1)^\nu = +1$. With interaction, at large U limit with small J, the system enters the xy-AFM phase [19,62,67]. With large J, interlayer dimer-singlet insulator is naturally the ground state of the BKMH-J model. The U-J phase diagram determined from the QMC simulations is presented in Fig. 7(b) for $\lambda = 0.2t$.

As demonstrated in Refs. [62,63], the BKMH-J model with $U = 0$ has an $SO(4) \simeq SU(2) \times SU(2)$ symmetry. To see it more clearly, we define $f_{i\uparrow} = (c_{1i\uparrow}, (-1)^i c^\dagger_{2i\uparrow})^T$ and $f_{i\downarrow} = ((-1)^i c_{1i\downarrow}, c^\dagger_{2i\downarrow})^T$, then the $SO(4)$ symmetry of BKMH-J model at $U = 0$ becomes explicit, since we can rewrite the model Hamiltonian with $\hat{P}_i = \frac{1}{2}(-1)^i \sum_\sigma f^\dagger_{i\sigma} i\tau^2 (f^\dagger_{i\sigma})^{\mathrm{T}}$ as

$$H = \sum_{i,j,\sigma} \chi_\sigma (f^\dagger_{i\sigma} t_{ij} f_{j\sigma} + \text{H.c.}) - \frac{J}{4} \sum_i (\hat{P}^\dagger_i \hat{P}_i + \hat{P}_i \hat{P}^\dagger_i), \quad (4)$$

where we have $\chi_\sigma = (-1)^\sigma$, and $t_{ij} = t$ for hoppings on the NN bonds and $t_{ij} = i\lambda$ for SOC on the next-nearest-neighbor (NNN) bonds. The Hamiltonian in Eq. (4) is invariant under the transformation: $f_{i\sigma} \to U_\sigma f_{i\sigma}$ with $U_\sigma \in SU(2)$ for both $\sigma = \uparrow, \downarrow$, so the BKHM-$J$ model at $U = 0$ indeed has the $SO(4) \simeq SU(2) \times SU(2)$ symmetry. This $SO(4)$ symmetry results in the degeneracy of interlayer spin-singlet s-wave pairing order and the interlayer xy-AFM order [62,63], such that both the interlayer spin-singlet s-wave pairing gap and the interlayer spin gap close at the J-driven TPT point denoted by the red point in Fig. 7(b).

Here we focus on the J-driven TPT at $U = 0$, as denoted by the blue line with arrow in Fig. 7(b). From the QMC results in Ref. [62], at the J-driven TPT point, both spin and charge gap close but the single-particle gap remains open, i.e., the fermionic degree of freedom is gapped out throughout the entire J axis. This is in sharp contrast with the interaction-driven TPTs in both GKMH (Sec. II A) and CKMH (Sec. II B) models, as well as those one-body-parameter-driven TPTs discussed in paper I [1]. This unique property means that this TPT has no free fermion correspondence.

What is the situation if we still perform the spin Chern number calculation based on single-particle Green's function as in GKMH (Sec. II A) and CKMH (Sec. II B) models? At $U = 0$ with increasing J, the QMC results of Chern number $C_\uparrow$ for $L = 6$ and $L = 12,18$ systems and the interpolation results with large $1/L$ are presented in Figs. 8(a) and 8(b). As expected, the $L = 6$, 12, and 18 results suffer severe finite-size effect and $C_\uparrow$ is much smaller than expected $C_s = +2$ even for very small J. After the interpolation with large $1/L$, the ideally quantized $C_\uparrow$ are obtained in both Figs. 8(a) and 8(b), but a very unexpected behavior appears: The $C_\uparrow$ constructed from single-particle Green's function do not change across this J-driven TPT. Correspondingly, we also observe that there is no parity change in any of the TRI points, and we find that the single-particle gap is also finite at the transition point, but it is the interlayer singlet pairing gap and interlayer spin

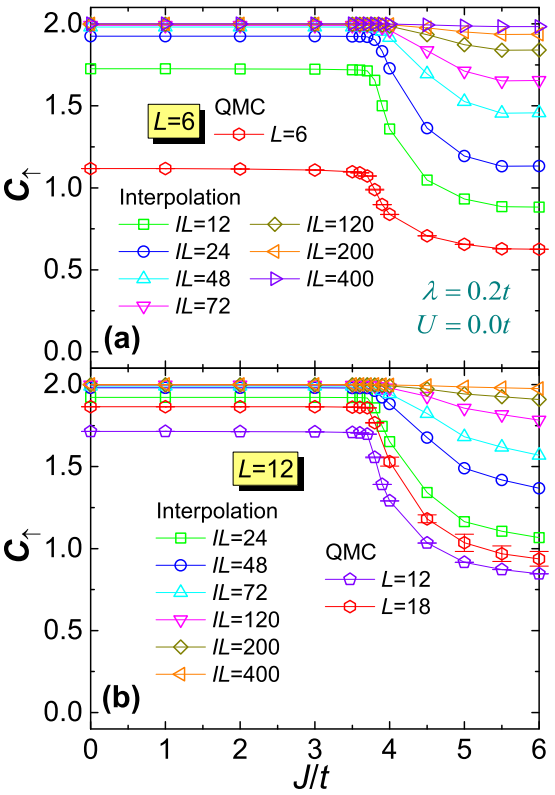

FIG. 8. Chern number $C_\uparrow$ for the J-driven TPT in the BKMH-J model with $\lambda = 0.2t, U = 0$ [the blue line with arrow in Fig. 7(b)] from QMC with $L = 6$, 12 and 18 and interpolation process, using the QMC data in (a) $L = 6$ and (b) $L = 12$ systems. The ideally quantized Chern number $C_\uparrow$ in large IL cases indicate that it has no variation across the J-driven TPT.

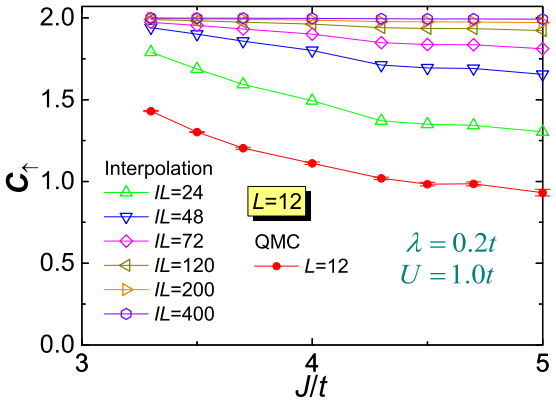

FIG. 9. Chern number $C_\uparrow$ for the finite-U inside the $SO(4)$ J-singlet insulator phase in BKMH-J model with $\lambda = 0.2t, U = 1$ [the magenta line with arrow in Fig. 7(b)] from both finite-size QMC calculation and interpolation process, using the QMC data of $L = 12$ systems. Chern number $C_\uparrow$ converges to $C_\uparrow = +2$ with increasing IL.

gap that close at the critical point $J_c \simeq 3.73$, as shown in Ref. [62]. From Fig. 8, it's really obscure to determine whether there is a J-driven $C_s = +2$ to $C_s = 0$ transition. Yet, we know that when $J > J_c$, the system is inside the interlayer dimer-singlet insulator phase without any edge states [62], as it is a direct product state of interlayer J singlets, under large-J limit. This seemingly contradicting result actually points out that the spin Chern number constructed from Green's function fails in detecting the J-driven TPT in the BKMH-J model. Actually, the same results of spin Chern number have also been obtained in Ref. [61] with finite frequency single-particle Green's function. This failure of spin Chern number is closely related to the interlayer dimer-singlet insulator phase, which has no free fermion correspondence, as well as the special nature of this TPT, i.e., it is the collective bosonic modes that become critical at the transition whereas the fermionic degree is always gapped [62].

To further illustrate the breakdown of the spin Chern number constructed from Green's function formalism in the BKMH-J model, we also calculate $C_\uparrow$ inside the interlayer dimer-singlet insulator phase at finite U. In the U-J phase diagram presented in Fig. 7(b), we choose a path at $\lambda = 0.2t, U = t$ with $J \in [3.3, 5.0]$ [the magenta path in Fig. 7(b)]. The Chern number $C_\uparrow$ calculated directly from $L = 12$ QMC simulation and after the interpolation process are presented in Fig. 9. Again, for the finite-U region inside the interlayer dimer-singlet insulator phase, spin Chern number C_s defined from single-particle Green's function possesses a $C_s = +2$ value, which is indeed unexpected. Regardless of $U = 0$ or $U \neq 0$, the interlayer dimer-singlet insulator phase should be topologically trivial (which has been confirmed by the absence of edge states from strange correlator measurements in QMC [62]). So now, it is clear that the spin Chern number cannot correctly describe this J-driven TPT in the BKMH-J model.

The interlayer dimer-singlet insulator phase in the BKMH-J model is a Mott insulator without any spontaneous symmetry breaking, and the J-driven TPT is TI-to-Mott-insulator transition. Furthermore, the interlayer dimer-singlet insulator phase cannot be adiabatically connected to any noninteracting band insulator without phase transition and symmetry breaking. This is in sharp contrast with the cases in both Sec. II A and Sec. II B, where the dimer insulator phase in the GKMH model and pVBS, cVBS phases in the CKMH model after the U-driven TPTs have their respective noninteracting correspondences. At first glance, one might think that at the $J \to \infty$ limit, the J-singlet phase is also adiabatically connected to a noninteracting insulator with large interlayer hopping t_z. Surely, a large t_z can give rise to a trivial band insulator. However, these two phases actually have different charge symmetries, which are $U(1) \times U(1)$ for the J-singlet phase and only a single $U(1)$ for the large-t_z insulator phase, respectively. According to this analysis, the nonexistent adiabatic connection to a band insulator is the essential reason for the breakdown of spin Chern number to capture the interlayer dimer-singlet insulator phase in the BKMH-J model.

D. Interaction-driven TPT in the BKMH-V model

The BKMH-J model is not a special case for the breakdown of the Green's function formalism of topological invariants. As proposed in Ref. [63], there are a series of interaction-driven TPT in 2D interacting TIs, where the single-particle gap does not close at the transition, and there is no noninteracting

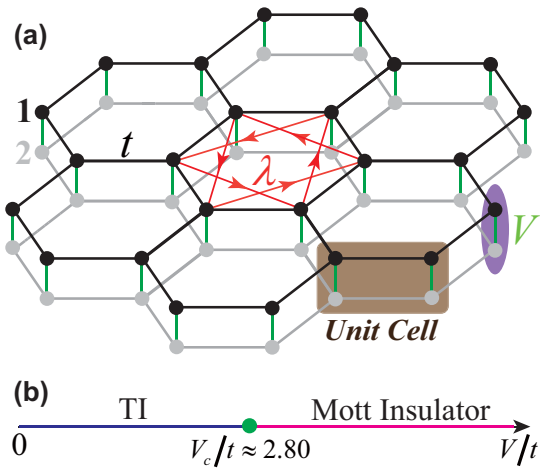

FIG. 10. (a) Illustration of the BKMH-V model. All the terms in Eq. (5) are identical to those in Eq. (3) except the interlayer AFM interaction J is replaced by the interlayer electron repulsion V. (b) The phase diagram of BKMH-V model. V-driven TPT from 2D TI to the featureless Mott insulator is at $V_c/t \simeq 2.80$.

correspondence for both the TPT itself and the topological trivial insulator phase after the transition. The bilayer Kane-Mele-Hubbard model with interlayer interaction V (BKMH-V model) in this section is the second explicit example.

The Hamiltonian is given as

$$\begin{aligned} H = & -t \sum_{\xi\langle i,j\rangle,\alpha} (c^\dagger_{\xi i\alpha} c_{\xi j\alpha} + c^\dagger_{\xi j\alpha} c_{\xi i\alpha}) \\ & + i\lambda \sum_{\xi\langle\langle i,j\rangle\rangle,\alpha\beta} v_{ij} (c^\dagger_{\xi i\alpha} \sigma^z_{\alpha\beta} c_{\xi j\beta} - c^\dagger_{\xi j\beta} \sigma^z_{\beta\alpha} c_{\xi i\alpha}) \\ & + V \sum_i (c^\dagger_{1i\uparrow} c_{2i\uparrow} c^\dagger_{1i\downarrow} c_{2i\downarrow} + c^\dagger_{2i\downarrow} c_{1i\downarrow} c^\dagger_{2i\uparrow} c_{1i\uparrow}), \end{aligned} \quad (5)$$

where both the lattice geometry and the model parameters are depicted in Fig. 10(a). The V interaction is actually pair hopping from one layer to the other, which is one of the most important terms from second quantization of Coulomb interaction. At first glance, this model preserves $[U(1) \times U(1)]_{\text{spin}} \times U(1)_{\text{charge}} \rtimes Z_2^T$ symmetry. Here the two $U(1)$ spin symmetries correspond to the S_z conservations in each layer. A more careful analysis reveals that this model also preserves the $SO(4) \simeq SU(2) \times SU(2)$ symmetry similar to the BKMH-J model at $U = 0$ in Sec. II C, since the model Hamiltonian in Eq. (5) can also be written by the f fermions as

$$H = \sum_{i,j,\sigma} \chi_\sigma (f^\dagger_{i\sigma} t_{ij} f_{j\sigma} + \text{H.c.}) - \frac{V}{2} \sum_i (\hat{P}_i \hat{P}_i + \hat{P}^\dagger_i \hat{P}^\dagger_i), \quad (6)$$

where χ_σ, t_{ij}, and $\hat{P}_i$ are all the same as those in Eq. (4). This Hamiltonian is also invariant under the transformation as $f_{i\sigma} \to U_\sigma f_{i\sigma}$ with $U_\sigma \in SU(2)$ for $\sigma = \uparrow, \downarrow$, independently, so the BKHM-V model indeed has the $SO(4) \simeq SU(2) \times SU(2)$ symmetry.

At $V \to \infty$ limit, one can actually obtain the exact many-body ground state wave function of Eq. (6), which is a direct product state as

$$|\Psi_g\rangle = \prod_i |\Psi_i\rangle = \prod_i \frac{1}{\sqrt{2}} (c^\dagger_{1i\uparrow} c^\dagger_{1i\downarrow} - c^\dagger_{2i\uparrow} c^\dagger_{2i\downarrow}) |0\rangle. \quad (7)$$

This ground state $|\Psi_g\rangle$ is indeed a featureless Mott insulator. It does not break the underlying $SO(4)$ symmetry of the Hamiltonian explicitly or spontaneously, as all the bilinear fermion condensations vanish. For example, one can easily verify that $\langle\Psi_g|c^\dagger_{\xi i\alpha} c_{\eta j\beta}|\Psi_g\rangle = \frac{1}{2}\delta_{\xi\eta}\delta_{ij}\delta_{\alpha\beta}$ and $\langle\Psi_g|c^\dagger_{\xi i\alpha} c^\dagger_{\eta j\beta}|\Psi_g\rangle = \langle\Psi_g|c_{\xi i\alpha} c_{\eta j\beta}|\Psi_g\rangle = 0$. What's more, $|\Psi_g\rangle$ does not have noninteracting correspondence either since one can simply observe the double occupancy of $|\Psi_g\rangle$ is $\langle\Psi_g|n_{1i\uparrow} n_{1i\downarrow}|\Psi_g\rangle = \langle\Psi_g|n_{2i\uparrow} n_{2i\downarrow}|\Psi_g\rangle = \frac{1}{2}$, whereas the double occupancy for a noninteracting system is $\frac{1}{4}$. Hence, the ground state $|\Psi_g\rangle$ in Eq. (7) for the model in Eq. (5) under $V \to +\infty$ limit is a featureless Mott insulator.

Our QMC results of the BKMH-V model reveal that there is a V-driven TPT from TI to Mott insulator at $V_c/t \simeq 2.82$. The corresponding phase diagram is presented in Fig. 10(b). We also confirm that the single-particle gap does not close across this TPT. Instead, the charge $2e$ excitation gap, corresponding to the on-site spin-singlet s-wave pairing order $\hat{\Delta}^\dagger_i = \frac{1}{\sqrt{2}}(c^\dagger_{1i\uparrow} c^\dagger_{1i\downarrow} - c^\dagger_{2i\uparrow} c^\dagger_{2i\downarrow})$, closes at the transition point. Both the single-particle gap and the on-site pairing gap across the topological phase transition for the BKMH-V model are presented in Appendix. After the transition, the system enters into a featureless Mott insulating phase.

To demonstrate the breakdown of the Green's function formalism across this V-driven TPT, we calculate the spin Chern number C_s for the BKMH-V model. The results of $C_\uparrow$ from QMC simulations of $L = 6, 12$ are presented in Figs. 11(a) and 11(b). Again, we can observe that $C_\uparrow$ varies continuously without finite-value jump for both $L = 6$ and $L = 12$ systems. By further applying the interpolation process to the data of $L = 6, 12$ systems, we obtain the integer-quantized Chern number $C_\uparrow$, also presented in Figs. 11(a) and 11(b). Same as the one in the BKMH-J model, the Chern number $C_\uparrow$ acquires no change across the V-driven TPT, since the $SO(4)$ V-singlet insulator at $V > V_c$ is a product state with all the electron degrees of freedom frozen, i.e., no edge states. The ideally quantized spin Chern number inside the featureless Mott insulator phase is another manifestation of the failure of the topological invariants constructed from the Green's function formalism.

III. HOW THE SPIN CHERN NUMBER WORKS

Based on the above QMC results in Secs. II A, II B, II C, and II D on interaction-driven topological phase transitions, we can now arrive at some basic understanding on the reason why the spin Chern number constructed from single-particle Green's function works well in some interacting topological quantum phases while it experiences breakdown in the others.

A. Working condition of the spin Chern number

In the interaction-driven TPTs in GKMH (Sec. II A) and CKMH (Sec. II B) models, all the phases can be adiabatically connected to the corresponding noninteracting insulator

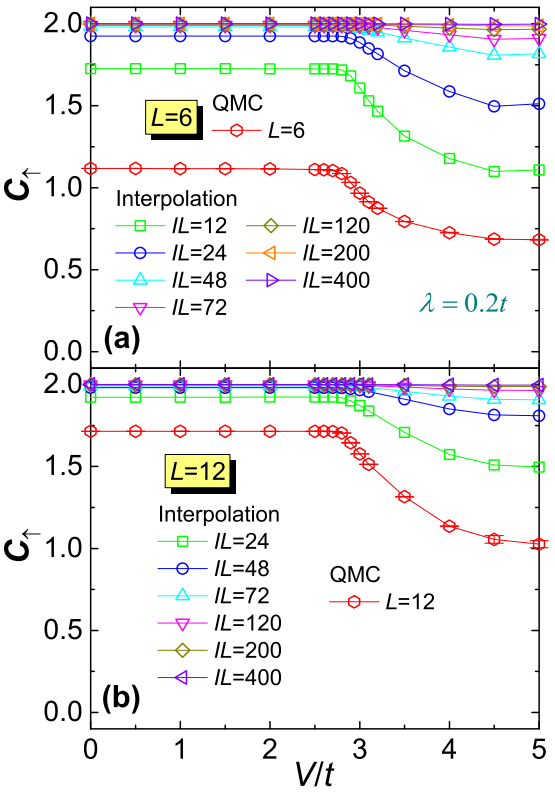

FIG. 11. Chern number $C_\uparrow$ for the V-driven TPT in the BKMH-V model with $\lambda = 0.2t$ from QMC and interpolation results using the QMC data in (a) $L = 6$ and (b) $L = 12$ systems. The ideally quantized Chern number $C_\uparrow$ in large IL cases indicate that $C_\uparrow$ has no variation across this topological phase transition.

phases in the same model Hamiltonian, and at the transitions, the single-particle gap closes, just like in the corresponding noninteracting cases. In these cases, the spin Chern number can be successfully applied to characterize topologically distinct phases and the TPTs. The underlying physics goes as follows. For the spin Chern number C_s constructed from the single-particle Green's function to acquire a change of integer number, the zero-frequency single-particle Green's function must possess either a pole or a zero [1]. The appearance of a pole corresponds to the single-particle gap closing, as observed in all the topological phase transitions in free fermion systems. The appearance of a zero in the single-particle Green's function across TPT has been discussed and found in interacting TIs [18,61,70]. Here, we have confirmed that the single-particle gap close at the U-driven TPTs in both GKMH and CKMH models. As for the J-driven TPT in BKMH-J and V-driven TPT in BKMH-V models, we find that across the transition, the single-particle gap keeps finite and there is neither pole nor zero appearing in the zero-frequency single-particle Green's function.

For a noninteracting TI with finite spin Chern number C_s, its spin Hall conductivity is $\sigma_{xy}^{spin} = C_s \frac{e^2}{h}$. For the free fermion system, the spin Chern number can be calculated from the single-particle Green's function [5–7,9]. For an interacting TI with finite C_s, if it is adiabatically connected to a noninteracting TI without phase transition and symmetry breaking, then this interacting TI should have exactly the same physical spin Hall conductivity. So we can conclude that in interacting systems if both phases across a TPT (driven by interaction or one-body-parameter and without explicit or spontaneous symmetry breaking) can be adiabatically connected to their noninteracting correspondences, then the spin Chern number calculated from single-particle Green's function can always characterize them and the transition.

B. Breakdown of the spin Chern number constructed from the Green's function

The reason for the breakdown of the spin Chern number constructed from the Green's function in the BKMH-J (Sec. II C) and BKMH-V (Sec. II D) models is twofold. First, the interlayer dimer-singlet insulator in BKMH-J model and the featureless Mott insulator in BKMH-V model after the transitions are Mott insulators without noninteracting correspondence. Second, the critical fluctuation associated to the transition is collective and bosonic instead of single-particle and fermionic.

Across the transition, neither pole nor zero of single-particle Green's function appears, which results in the same integer values of the spin Chern number. In the interlayer dimer-singlet insulator and featureless Mott insulator phase, as shown in Figs. 8, 9, and 11, the spin Chern number constructed from the single-particle Green's function is equal to $C_s = +2$, which is an artifact of the Green's function formalism.

We can understand such an artifact from the perspective of symmetry-protected topological (SPT) phases [58,59]. An important property of SPTs is that they only have short-range entanglement and can be adiabatically connected to some direct product state (with the same topological invariant) without going through symmetry breaking and phase transitions. The simplest product state for noninteracting fermion systems is the Slater determinant, i.e., a product state of free fermion wave function in momentum space. The noninteracting correspondences of the trivial insulators after the U-driven TPTs in GKMH and CKMH models are such Slater determinants. However, for BKMH-J and BKMH-V models, although the interlayer dimer-singlet insulator and featureless Mott insulator at large J and V can be adiabatically connected to the product states at the limit of $J \to +\infty$ and $V \to +\infty$, the wave-function basis of such product states are singlets consisting of two electrons [71], instead of the single-electron wavefunction used to construct the Slater determinant. Thus, the interlayer dimer-singlet insulator and featureless Mott insulator in BKMH-J and BKMH-V models are not adiabatically connected to free-fermion Slater determinants. In the cases of BKMH-J and BKMH-V models, even if one constructs the topological invariants from single-particle Green's function formalism, the obtained spin Chern numbers do not correspond to the physical spin Hall conductivity. The physical spin Hall conductivity, on the other hand, should be carried by the emergent low-energy bosonic modes, which become critical at these interaction-driven TPTs [62,63].

IV. SUMMARY

By means of large-scale QMC simulations, we have investigated several interaction-driven topological phase

transitions in 2D interacting TIs without explicit or spontaneous symmetry breaking. We further characterize these TPTs via the topological invariants across these interaction-driven TPTs, including Z_2 invariant and spin Chern number constructed from single-particle Green's function at zero frequency. We find that the spin Chern number successfully detects the interaction-driven TPTs in GKMH (Sec. II A) and CKMH (Sec. II B) models, while it experiences unexpected breakdown in BKMH-J (Sec. II C) and BKMH-V (Sec. II D) models. To understand such breakdown, we have analyzed the working condition for spin Chern number constructed in Green's function formalism, and discuss why it fails for the interlayer dimer-singlet insulator and featureless Mott insulator phases in BKMH-J and BKMH-V models. It turns out that the spin Chern number constructed from single-particle Green's function can only characterize interacting TIs which can be adiabatically connected to noninteracting insulators, for which the spin Chern number corresponds to the physical spin Hall conductivity. For interacting TIs without noninteracting correspondence, the spin Chern number constructed from single-particle Green's function is artificial, as demonstrated in BKMH-J and BKMH-V models.

In terms of SPT, the interlayer dimer-singlet insulator and the featureless Mott insulator in BKMH-J and BKMH-V models, where the spin Chern number experiences breakdown, are indeed SPT trivial states. Actually, the interaction-driven TPTs in these models are of bosonic nature due to the gapped fermion degree of freedom. Our work highlights the important issue of how to characterize the topological aspects of SPT states in generally interacting fermion systems which cannot be adiabatically connected a noninteracting band insulator. As a result, we expect new and more versatile techniques to correctly describe the topological invariants in such interacting states. Recent progress in calculating entanglement spectrum [72,73], entanglement entropy [74], and directly probing the edge states via strange correlation [68,75] in interacting TIs seem to provide promising directions.

ACKNOWLEDGMENTS

We thanks Yi-Zhuang You, Lei Wang, Ning-Hua Tong, Zheng-Xin Liu, Zhong Wang, Cenke Xu, Liang Fu, Kai Sun, and Xi Dai for inspiring discussions on various aspects of this paper. The numerical calculations were carried out at the Physical Laboratory of High Performance Computing in Renmin University of China, the supercomputing platforms in the Center for Quantum Simulation Sciences in the Institute of Physics, Chinese Academy of Sciences, as well as the National Supercomputer Center in TianJin on the platform Tianhe-1A. Y.Y.H., H.Q.W., Z.Y.M., and Z.Y.L. acknowledge support from National Natural Science Foundation of China (Grants No. 91421304, No. 11474356, No. 11421092, and No. 11574359). Z.Y.M. is also supported by the National Thousand-Young-Talents Program of China, and acknowledges the hospitality of the KITP at the University of California, Santa Barbara, where part of this work is initiated.

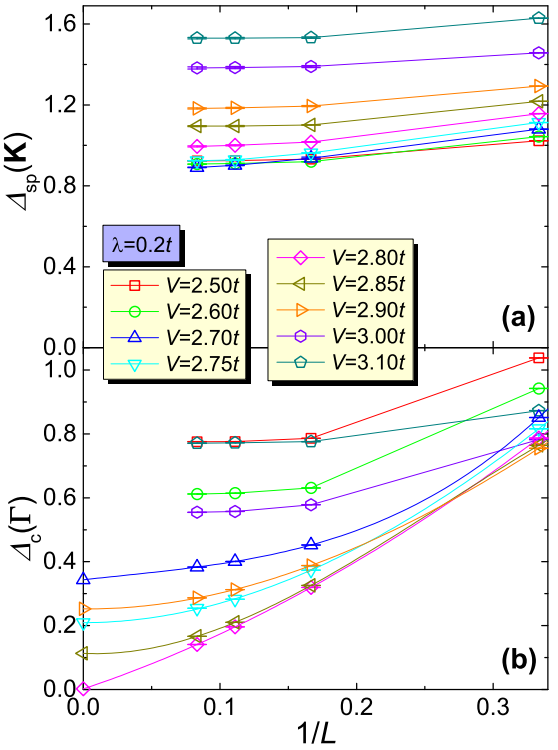

FIG. 12. (a) Single-particle gap $\Delta_{sp}(\mathbf{K})$ and (b) charge gap $\Delta_c(\Gamma)$ for the BKMH-V model with $\lambda = 0.2t$ for chosen $V/t = 2.5 \sim 3.1$. $\Delta_{sp}(\mathbf{K})$ keeps finite across the TPT, while $\Delta_c(\Gamma)$ experiences a closing and reopening at $V_c/t \simeq 2.80$ after the extrapolation to thermodynamic with third-order polynomial in $1/L$.

APPENDIX: EXCITATION GAPS ACROSS THE TPT IN THE BKMH-V MODEL

For BKMH-V model in Eq. (5), we have mentioned that the single-particle gap keeps finite while the charge gap (on-site pairing gap) closes and reopens across the topological phase transition, at $V_c/t \simeq 2.80$. Here, we present numerical data of both gaps for the BKMH-V model.

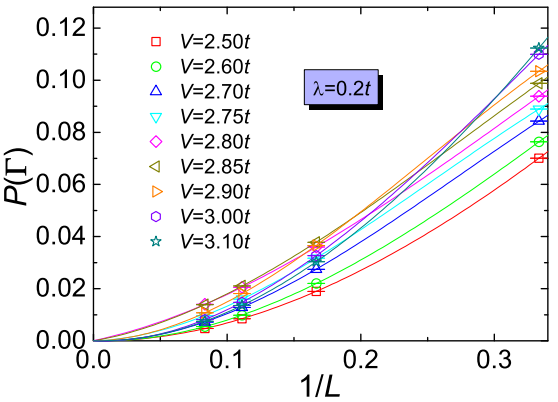

FIG. 13. Structure factor $P(\Gamma)/N$ and its finite-size extrapolation over $1/L$ by cubic polynomials for the on-site spin-singlet s-wave superconductivity order in Eq. (A1) for $L = 3,6,9,12$ with $V/t = 2.5 \sim 3.1$. From the results, the superconductivity order is always short-ranged in the BKMH-V model.

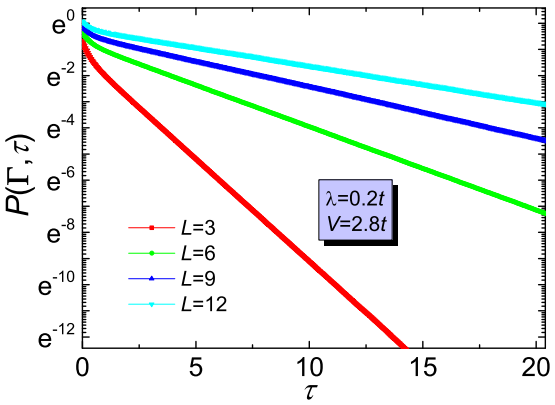

FIG. 14. Original data of $[P(\Gamma,\tau)]_{11}$ at topological phase transition point $V/t = 2.80$ for BKMH-V model systems with $L = 3,6,9,12$, under semilogarithmic plot.

The single-particle gap is extracted from the imaginary-time single-particle Green's function in reciprocal space as $G_\sigma(\tau,\mathbf{k})$, which is a 4×4 Hermitian matrix for the BKMH-V model. At the $\tau\to+\infty$ limit, we have $[G_\sigma(\tau,\mathbf{k})]_{\alpha\alpha}\propto Z_{\mathbf{k}}e^{-\tau\Delta_{sp}(\mathbf{k})}$ with $\alpha=1,2,3,4$ indicating sublattices, and $\Delta_{sp}(\mathbf{k})$ is the single-particle gap at $\mathbf{k}$ point for the system. As for the on-site pairing gap, we define the spin-singlet s-wave pairing order

$$\hat{\Delta}^\dagger_{i\alpha}=\frac{1}{\sqrt{2}}(c^\dagger_{1i\alpha\uparrow}c^\dagger_{1i\alpha\downarrow}-c^\dagger_{2i\alpha\uparrow}c^\dagger_{2i\alpha\downarrow}), \tag{A1}$$

where $\alpha=1,2$ stands for A,B sublattices respectively and integer i represents the unit cells of the bilayer model. One can observe that $\hat{\Delta}^\dagger_{i\alpha}$ represents local pairing order on vertical bonds between layers. Then we can obtain the dynamic correlation function in reciprocal space for such on-site pairing order as

$$[P(\mathbf{Q},\tau)]_{\alpha\beta}=\frac{1}{N}\sum_{ij}e^{i\mathbf{Q}\cdot(\mathbf{R}_i-\mathbf{R}_j)}\langle T_\tau[\hat{\Delta}^\dagger_{i\alpha}(\tau)\hat{\Delta}_{j\beta}(0)]\rangle, \tag{A2}$$

where $\mathbf{Q}=\Gamma$ is the ordering vector for the BKMH-V model and $N=L^2$ is the number of unit cells for a $L\times L$ system. Then we can extract the corresponding charge gap $\Delta_c(\mathbf{Q})$ under $\tau\to+\infty$ limit via $[P(\mathbf{Q},\tau)]_{\alpha\alpha}\propto R_{\mathbf{Q}}e^{-\tau\Delta_c(\mathbf{Q})}$.

Both the numerical results of single-particle gap $\Delta_{sp}(\mathbf{K})$ and charge gap $\Delta_c(\Gamma)$ across the TPT in the BKMH-V model with $\lambda=0.2t$ are shown in Fig. 12. The single-particle gap $\Delta_{sp}(\mathbf{K})$ [Fig. 12(a)] keeps finite with a large value at the $L\to\infty$ limit, which is about $0.9t$ at the topological phase transition point. However, the charge gap $\Delta_c(\Gamma)$ acquires a closing and reopening across the TPT around $V_c/t\simeq 2.80$.

To exclude the possible stepping in of long-range on-site spin-singlet s-wave superconductivity order, we have calculated the structure factors $P(\Gamma)$ for the order in Eq. (A1) for $L=3,6,9,12$ systems. The result and its finite-size extrapolation over $1/L$ to thermodynamic limit are shown in Fig. 13. One can observe that the superconductivity order is always short-ranged in the BKMH-V model. Combining with the excitation gaps result, it's clear that the pairing gap closing and reopening at the topological phase transition point is an intrinsic property of the model.

We emphasize that the original data of $[P(\Gamma,\tau)]_{11}$, via which we extract the charge gap $\Delta_c(\Gamma)$, has quite high quality. For example, we present $[P(\Gamma,\tau)]_{11}$ data for $V/t=2.80$ in BKMH-V model systems with $L=3,6,9,12$ in Fig. 14 with semilogarithmic plot. In Fig. 14, we can see that the data of $\ln[P(\Gamma,\tau)]_{11}$ is perfectly linear with imaginary-time τ. Thus, the closing of charge gap $\Delta_c(\Gamma)$ around $V_c/t\simeq 2.80$ at the V-driven topological phase transition point in the BKMH-V model, as shown in Fig. 12(b), is sufficiently solid.

[1] Y.-Y. He, H.-Q. Wu, Z. Y. Meng, and Z.-Y. Lu, Phys. Rev. B **93**, 195163 (2016).
[2] C. L. Kane and E. J. Mele, Phys. Rev. Lett. **95**, 146802 (2005).
[3] L. Fu and C. L. Kane, Phys. Rev. B **76**, 045302 (2007).
[4] E. Prodan, Phys. Rev. B **80**, 125327 (2009).
[5] G. E. Volovik, *The Universe in a Helium Droplet* (Oxford University Press, New York, 2009).
[6] J. E. Avron, R. Seiler, and B. Simon, Phys. Rev. Lett. **51**, 51 (1983).
[7] H. So, Prog. Theor. Phys. **74**, 585 (1985).
[8] K. Ishikawa and T. Matsuyama, Z. Phys. C **33**, 41 (1986).
[9] G. E. Volovik, JETP **67**, 1804 (1988).
[10] Z. Wang, X.-L. Qi, and S.-C. Zhang, Phys. Rev. Lett. **105**, 256803 (2010).
[11] V. Gurarie, Phys. Rev. B **83**, 085426 (2011).
[12] Q. Niu, D. J. Thouless, and Y.-S. Wu, Phys. Rev. B **31**, 3372 (1985).
[13] Z. Wang and S.-C. Zhang, Phys. Rev. X **4**, 011006 (2014).
[14] Z. Wang, X.-L. Qi, and S.-C. Zhang, Phys. Rev. B **84**, 014527 (2011).
[15] Z. Wang, X.-L. Qi, and S.-C. Zhang, Phys. Rev. B **85**, 165126 (2012).
[16] Z. Wang and S.-C. Zhang, Phys. Rev. B **86**, 165116 (2012).
[17] Z. Wang and S.-C. Zhang, Phys. Rev. X **2**, 031008 (2012).
[18] T. Yoshida, R. Peters, S. Fujimoto, and N. Kawakami, Phys. Rev. Lett. **112**, 196404 (2014).
[19] Z. Y. Meng, H.-H. Hung, and T. C. Lang, Mod. Phys. Lett. B **28**, 1430001 (2014).
[20] H.-H. Hung, L. Wang, Z.-C. Gu, and G. A. Fiete, Phys. Rev. B **87**, 121113 (2013).
[21] H.-H. Hung, V. Chua, L. Wang, and G. A. Fiete, Phys. Rev. B **89**, 235104 (2014).
[22] Y.-H. Chen, H.-H. Hung, G. Su, G. A. Fiete, and C. S. Ting, Phys. Rev. B **91**, 045122 (2015).
[23] F. Grandi, F. Manghi, O. Corradini, and C. M. Bertoni, Phys. Rev. B **91**, 115112 (2015).
[24] T. Yoshida, S. Fujimoto, and N. Kawakami, Phys. Rev. B **85**, 125113 (2012).
[25] J. C. Budich, B. Trauzettel, and G. Sangiovanni, Phys. Rev. B **87**, 235104 (2013).
[26] A. Amaricci, J. C. Budich, M. Capone, B. Trauzettel, and G. Sangiovanni, Phys. Rev. Lett. **114**, 185701 (2015).
[27] F. Lu, J. Z. Zhao, H. Weng, Z. Fang, and X. Dai, Phys. Rev. Lett. **110**, 096401 (2013).

[28] X. Deng, K. Haule, and G. Kotliar, Phys. Rev. Lett. **111**, 176404 (2013).
[29] M. Dzero, K. Sun, V. Galitski, and P. Coleman, Phys. Rev. Lett. **104**, 106408 (2010).
[30] J. Jiang, S. Li, T. Zhang, Z. Sun, F. Chen, Z. R. Ye, M. Xu, Q. Q. Ge, S. Y. Tan, X. H. Niu, M. Xia, B. P. Xie, Y. F. Li, X. H. Chen, H. H. Wen, and D. L. Feng, Nat. Commun. **4**, 3010 (2013).
[31] N. Xu, P. K. Biswas, J. H. Dil, R. S. Dhaka, G. Landolt, S. Muff, C. E. Matt, X. Shi, N. C. Plumb, M. Radovic, E. Pomjakushina, K. Conder, A. Amato, S. V. Borisenko, R. Yu, H.-M. Weng, Z. Fang, X. Dai, J. Mesot, H. Ding, and M. Shi, Nat. Commun. **5**, 4566 (2014).
[32] D. A. Pesin and L. Balents, Nat. Phys. **6**, 376 (2010).
[33] J. Maciejko and G. A. Fiete, Nat. Phys. **11**, 385 (2015).
[34] A. Kitaev, AIP Conf. Proc. **1134**, 22 (2009).
[35] A. P. Schnyder, S. Ryu, A. Furusaki, and A. W. W. Ludwig, AIP Conf. Proc. **1134**, 10 (2009).
[36] S. Ryu, A. P. Schnyder, A. Furusaki, and A. W. W. Ludwig, New J. Phys. **12**, 065010 (2010).
[37] L. Fidkowski and A. Kitaev, Phys. Rev. B **81**, 134509 (2010).
[38] L. Fidkowski and A. Kitaev, Phys. Rev. B **83**, 075103 (2011).
[39] S. Ryu and S.-C. Zhang, Phys. Rev. B **85**, 245132 (2012).
[40] Y.-M. Lu and A. Vishwanath, Phys. Rev. B **86**, 125119 (2012).
[41] X.-L. Qi, New J. Phys. **15**, 065002 (2013).
[42] H. Yao and S. Ryu, Phys. Rev. B **88**, 064507 (2013).
[43] L. Fidkowski, X. Chen, and A. Vishwanath, Phys. Rev. X **3**, 041016 (2013).
[44] C. Wang and T. Senthil, Phys. Rev. B **89**, 195124 (2014).
[45] Z.-C. Gu and M. Levin, Phys. Rev. B **89**, 201113 (2014).
[46] Y.-Z. You, Y. BenTov, and C. Xu, arXiv:1402.4151.
[47] Y.-Z. You and C. Xu, Phys. Rev. B **90**, 245120 (2014).
[48] Y.-Z. You and C. Xu, Phys. Rev. B **91**, 125147 (2015).
[49] T. Morimoto, A. Furusaki, and C. Mudry, Phys. Rev. B **92**, 125104 (2015).
[50] C. Wang and T. Senthil, Phys. Rev. B **87**, 235122 (2013).
[51] C. Wang, A. C. Potter, and T. Senthil, Phys. Rev. B **88**, 115137 (2013).
[52] P. Bonderson, C. Nayak, and X.-L. Qi, J. Stat. Mech. (2013) P09016.
[53] X. Chen, L. Fidkowski, and A. Vishwanath, Phys. Rev. B **89**, 165132 (2014).
[54] C. Wang, A. C. Potter, and T. Senthil, Science **343**, 629 (2014).
[55] M. A. Metlitski, C. L. Kane, and M. P. A. Fisher, Phys. Rev. B **92**, 125111 (2015).
[56] C. Wang and T. Senthil, Phys. Rev. X **5**, 041031 (2015).
[57] M. A. Metlitski and A. Vishwanath, arXiv:1505.05142.
[58] X. Chen, Z.-C. Gu, Z.-X. Liu, and X.-G. Wen, Science **338**, 1604 (2012).
[59] X. Chen, Z.-C. Gu, Z.-X. Liu, and X.-G. Wen, Phys. Rev. B **87**, 155114 (2013).
[60] Z.-X. Liu and X.-G. Wen, Phys. Rev. Lett. **110**, 067205 (2013).
[61] K. Slagle, Y.-Z. You, and C. Xu, Phys. Rev. B **91**, 115121 (2015).
[62] Y.-Y. He, H.-Q. Wu, Y.-Z. You, C. Xu, Z. Y. Meng, and Z.-Y. Lu, Phys. Rev. B **93**, 115150 (2016).
[63] Y.-Z. You, Z. Bi, D. Mao, and C. Xu, Phys. Rev. B **93**, 125101 (2016).
[64] W. Wu, S. Rachel, W.-M. Liu, and K. Le Hur, Phys. Rev. B **85**, 205102 (2012).
[65] M. Hohenadler, T. C. Lang, and F. F. Assaad, Phys. Rev. Lett. **106**, 100403 (2011).
[66] D. Zheng, G.-M. Zhang, and C. Wu, Phys. Rev. B **84**, 205121 (2011).
[67] M. Hohenadler, Z. Y. Meng, T. C. Lang, S. Wessel, A. Muramatsu, and F. F. Assaad, Phys. Rev. B **85**, 115132 (2012).
[68] H.-Q. Wu, Y.-Y. He, Y.-Z. You, C. Xu, Z. Y. Meng, and Z.-Y. Lu, Phys. Rev. B **92**, 165123 (2015).
[69] T. C. Lang, Z. Y. Meng, A. Muramatsu, S. Wessel, and F. F. Assaad, Phys. Rev. Lett. **111**, 066401 (2013).
[70] Y.-Z. You, Z. Wang, J. Oon, and C. Xu, Phys. Rev. B **90**, 060502 (2014).
[71] S.-Q. Ning, H.-C. Jiang, and Z.-X. Liu, Phys. Rev. B **91**, 241105 (2015).
[72] F. F. Assaad, T. C. Lang, and F. Parisen Toldin, Phys. Rev. B **89**, 125121 (2014).
[73] F. F. Assaad, Phys. Rev. B **91**, 125146 (2015).
[74] D. Wang, S. Xu, Y. Wang, and C. Wu, Phys. Rev. B **91**, 115118 (2015).
[75] Y.-Z. You, Z. Bi, A. Rasmussen, K. Slagle, and C. Xu, Phys. Rev. Lett. **112**, 247202 (2014).